
Article:
Balikhin, M. and Gedalin, M. (2022) Collisionless shocks in the heliosphere: Foot width revisited. The Astrophysical Journal, 925 (1). 90. ISSN: 0004-637X

https://doi.org/10.3847/1538-4357/ac3bb3

The Astrophysical Journal, 925:90 (7pp), 2022 January 20 https://doi.org/10.3847/1538-4357/ac3bb3

Collisionless Shocks in the Heliosphere: Foot Width Revisited

Michael Balikhin[1] and Michael Gedalin[2]
[1] University of Sheffield, Sheffield, UK; m.balikhin@sheffield.ac.uk
[2] Department of Physics, Ben Gurion University of the Negev, Beer-Sheva, Israel
Received 2021 September 10; revised 2021 October 21; accepted 2021 November 18; published 2022 January 27

Abstract

For single-point measurements of quasi-perpendicular shocks, analytical measurements of the foot width are often used to evaluate the velocity of the shock relative to the satellite. This velocity is of crucial importance for in situ observations because it enables the identification of the spatial scale of other regions of the shock front such as a magnetic ramp for which the comprehensive understanding of their formation is not yet achieved. Knowledge of the spatial scale is one of the key parameters for the validation of theoretical models that are developed to explain the formation of these regions. Previously available estimates of the foot width for a quasi-perpendicular shock are based on several simplifications such as zero upstream ion temperature and specular ion reflection by the cross-shock electrostatic potential. The occurrence of specular reflection implies high values of the cross-shock electrostatic potential that significantly exceed the values obtained from in situ measurements. In this paper the effects of nonzero ion temperature and nonspecular ion reflection on the foot width are investigated. It is shown that in the case of nonspecular reflection the foot width can be as small as half of the size of the standard widely used estimate. Results presented here enable more reliable identification of the shock velocity from single-point observations.

Unified Astronomy Thesaurus concepts: Shocks (2086)

1. Introduction

The main process that takes place at the front of a collisionless shock is the redistribution of the kinetic energy of the bulk plasma motion to plasma thermalization and the acceleration of a small fraction of plasma particles. Drastic changes in plasma parameters such as density, magnetic field, temperature, and others occur at the shock front. The spatial scales of these changes are important for the understanding of the nature of the shock, i.e., the dynamical processes that counterbalance the nonlinear steepening of the shock front and therefore lead to the formation of the front structure. In the case of supercritical quasi-perpendicular shocks, the spatial scales of the regions of the front such as the foot, the ramp, and overshoot are unambiguously related to the physics of their formation. It is generally understood that the formation of the foot (Woods 1971) and overshoot/undershoot (Livesey et al. 1982) regions is related to the ion motion within the shock front. Currently, there is no comprehensive understanding of what determines the width of the ramp (Krasnoselskikh et al. 2013). Observations from the four-point Cluster mission enable a complete separation between the observed spatial and temporal variations and therefore an unequivocal determination of the spatial scales of the observed phenomena. These multipoint data sets enable statistical studies of the spatial scale of the ramp for the quasi-perpendicular region of the terrestrial bow shock (Hobara et al. 2010). Currently, however, such in situ measurements obtained by four closely separated spacecraft (e.g., Cluster, THEMIS, MMS) are available only in the vicinity of Earth and are thus limited to studies of the terrestrial bow shock and interplanetary shocks at 1 au. Collisionless shocks are abundant in the universe and exist around ordinary stars, in binary systems, in supernova remnants, and in active galactic nuclei. However, only shocks within the heliosphere can be studied using in situ measurements. It is important to study all varieties of shocks available for in situ observations. The identification of "kinematic shocks" near Venus, which refuted the longstanding conjecture that the overshoot is an unambiguous sign of supercritical shock (Balikhin et al. 2008; Russell et al. 2009; Gedalin 2019; Pope et al. 2019; Pope 2020), is an example of why it is important to study heliospheric shocks in all their diversity. Currently no close separation multipoint measurements are available for planetary or solar missions. While a number of techniques have been used to identify the spatial scale of the shock front in the pre-ISEE era, the most often employed is the technique based on the spatial scale of the foot region. The first accurate estimate of the width of the foot region for a supercritical perpendicular shock was obtained by Woods (1971). It was further simplified by Phillips & Robson (1972) who assumed specular reflection and cold upstream ions. Livesey et al. (1984) extended the theory of Phillips & Robson (1972) to include quasi-perpendicular geometry. Their expression was used to identify the relative velocity of the Jovian shock with respect to the Voyager spacecraft (Moses et al. 1985). The expression for the foot width of a quasi-perpendicular shock was corrected by Gosling & Thomsen (1985) who took into account the reflected ion motion along the magnetic field in addition to the drift and gyration. Since then, the formula of Gosling & Thomsen (1985) has often been used for the determination of the shock speed in the spacecraft frame. However, this expression implies that the ions moving with the flow velocity are specularly reflected by the cross-shock potential. Such reflection requires high cross-shock potentials (Wilkinson & Schwartz 1990), which are not observed (Schwartz et al. 1988; Dimmock et al. 2012). In such cases, the fraction of reflected ions would be too large and a stationary shock could hardly exist. Neither observations (Sckopke et al. 1983, 1990) nor numerical simulations (Burgess et al. 1989) show such a strong reflection. In addition, the formula does not depend on parameters such as the shock Mach number (or the ratio of the Mach number M to the critical Mach M_{cr}) or

plasma β, and only assumes that ion reflection occurs. Ion reflection is also observed in low-Mach number shocks without an extended foot (Gedalin et al. 2018) and in high-Mach number reforming shocks, which means that the foot width should depend on the shock parameters.

In the current study we generalize the expression of Gosling & Thomsen (1985) and derive the positions of the turning points for specularly reflected ions with different initial velocities. We further numerically analyze the ion motion in a model shock profile with a realistic cross-shock potential and show that the expected foot widths can be as small as about a half of the Gosling & Thomsen (1985) estimate that is based on a specular reflection model.

2. Turning Point of a Specularly Reflected ion

The widely accepted estimate of the foot width (Schwartz et al. 1983; Gosling & Thomsen 1985) is based on several assumptions. First, the upstream fields are assumed uniform. The fields are

$$B_x = B_u\cos\theta_{Bn},\quad B_y = 0,\quad B_z = B_u\sin\theta_{Bn} \tag{1}$$

$$E_x = 0,\quad E_y = \frac{V_u}{c}B_z,\quad E_z = 0 \tag{2}$$

Here x is along the shock normal, y is the noncoplanarity direction, and θ_{Bn} is the angle between the shock normal and the upstream magnetic field direction. Second, it is assumed that an ion, which enters the shock with the fluid velocity, is specularly reflected by the cross-shock potential so during the reflection process the component of the ion velocity in the direction of the shock normal changes its sign while the tangential components remain unchanged. The analysis by Gosling & Thomsen (1985) is done in the de Hoffman–Teller (HT) frame, in which the upstream and downstream plasma velocities are aligned with the upstream and downstream magnetic fields, respectively. It is assumed that the ion moving with the flow velocity is specularly reflected. Below we perform a more general analysis in the normal incidence frame (NIF), in which the upstream plasma velocity is along the shock normal. In general, in these uniform fields, a particle moves along the magnetic field with velocity $v_\parallel$, gyrates around the magnetic field with speed $v_\perp$, and drifts with velocity $c\vec{E}\times\boldsymbol{B}/|\boldsymbol{B}|^2$. Let

$$\hat{b} = \frac{\boldsymbol{B}}{|\boldsymbol{B}|} = (\cos\theta_{Bn},\,0,\,\sin\theta_{Bn}) \tag{3}$$

$$\hat{e}_2 = \hat{y} = (0,\,1,\,0) \tag{4}$$

$$\hat{e}_1 = \hat{e}_2\times\hat{b} = (\sin\theta_{Bn},\,0,\,-\cos\theta_{Bn}) \tag{5}$$

$$\Omega = \frac{eB_u}{\mathrm{mc}},\quad \psi = \Omega t \tag{6}$$

then

$$\boldsymbol{v} = v_\parallel\hat{b} + (\sin\theta_{Bn} + v_\perp\cos(\psi-\phi))\hat{e}_1 - v_\perp\sin(\psi-\phi)\hat{e}_2 \tag{7}$$

$$v_x = v_\parallel\cos\theta_{Bn} + \sin^2\theta_{Bn} + v_\perp\sin\theta_{Bn}\cos(\psi-\phi) \tag{8}$$

$$v_y = -v_\perp\sin(\psi-\phi) \tag{9}$$

$$v_z = v_\parallel\sin\theta_{Bn} - \sin\theta_{Bn}\cos\theta_{Bn} - v_\perp\cos\theta_{Bn}\cos(\psi-\phi)) \tag{10}$$

$$X = (v_\parallel\cos\theta_{Bn} + \sin^2\theta_{Bn})\psi + v_\perp\sin\theta_{Bn}[\sin(\psi-\phi) + \sin\phi] \tag{11}$$

where all velocities are normalized to V_u, ϕ is the initial gyrophase and $X = \Omega x/V_u$. The initial conditions at $\psi = 0$ are

$$v_{x0} = v_\parallel\cos\theta_{Bn} + \sin^2\theta_{Bn} + v_\perp\sin\theta_{Bn}\cos\phi \tag{12}$$

$$v_{y0} = v_\perp\sin\phi \tag{13}$$

$$v_{z0} = v_\parallel\sin\theta_{Bn} - \sin\theta_{Bn}\cos\theta_{Bn} - v_\perp\cos\theta_{Bn}\cos\phi \tag{14}$$

which gives

$$v_\parallel = v_{x0}\cos\theta_{Bn} + v_{z0}\sin\theta_{Bn} \tag{15}$$

$$v_\perp\cos\phi = v_{x0}\sin\theta_{Bn} - v_{z0}\cos\theta_{Bn} - 1 \tag{16}$$

$$v_\perp\sin\phi = v_{y0} \tag{17}$$

$$v_\perp = [((v_{x0}-1)\sin\theta_{Bn} - v_{z0}\cos\theta_{Bn})^2 + v_{y0}^2]^{1/2} \tag{18}$$

$$\sin\phi = \frac{v_{y0}}{v_\perp} \tag{19}$$

$$\cos\phi = \frac{(v_{x0}-1)\sin\theta_{Bn} - v_{z0}\cos\theta_{Bn}}{v_\perp} \tag{20}$$

A reflected ion has

$$v_{x0} = v_\parallel\cos\theta_{Bn} + \sin^2\theta_{Bn} + v_\perp\sin\theta_{Bn}\cos\phi < 0 \tag{21}$$

It turns back toward the ramp when

$$v_x(\psi) = v_\parallel\cos\theta_{Bn} + \sin^2\theta_{Bn} + v_\perp\sin\theta_{Bn}\cos(\psi-\phi) = 0 \tag{22}$$

$$\cos(\psi-\phi) = -\frac{v_\parallel\cos\theta_{Bn} + \sin^2\theta_{Bn}}{v_\perp} \tag{23}$$

provided

$$|v_\parallel\cos\theta_{Bn} + \sin^2\theta_{Bn}| \leqslant v_\perp \tag{24}$$

We have also $\sin(\psi-\phi) < 0$, since at the turning point $\Omega v_y = dv_x/dt > 0$. The turning distance is then given by (11) where

$$\psi = \phi - \arccos\left(-\frac{v_\parallel\cos\theta_{Bn} + \sin^2\theta_{Bn}}{v_\perp}\right) \tag{25}$$

In this section we consider specular reflection in which a reflected ion changes the normal component of its velocity at its reflection point while the tangential components do not change. In addition, we neglect the ramp width and assume that any incident ion with $mv_x^2/2 < s(mV_u^2/2)$ is immediately reflected without any magnetic deflection. Here $s = 2e\phi/mV_u^2$ is the NIF cross-shock potential normalized to the kinetic energy of the bulk motion. Note that the calculation of the foot width as the turning distance of the ion moving at the fluid velocity implies

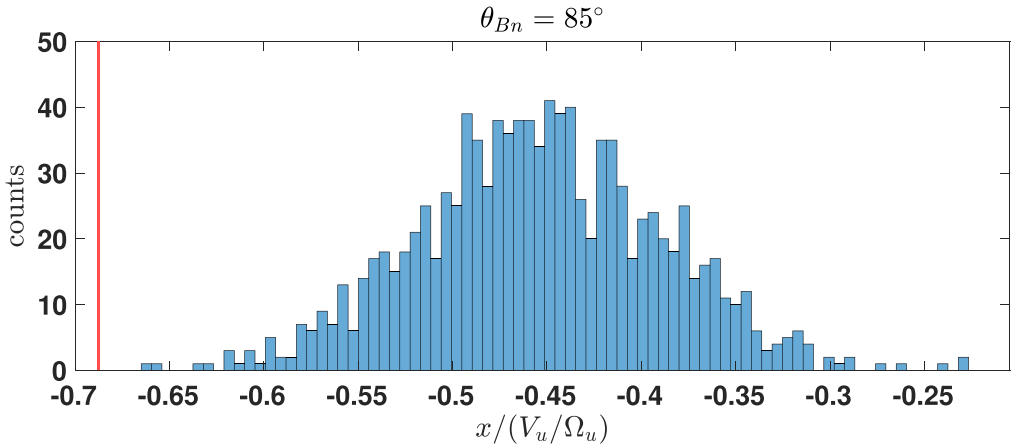

Figure 1. Histogram of the turning points of specularly reflected ions, given by (11) and (25), for an incident Maxwellian distribution. The parameters are: $\theta_{Bn} = 85^\circ$, $M = 4$, $\beta = 0.5$, $s = 0.6$. The red line marks the position of the upstream edge of the foot according to Gosling & Thomsen (1985).

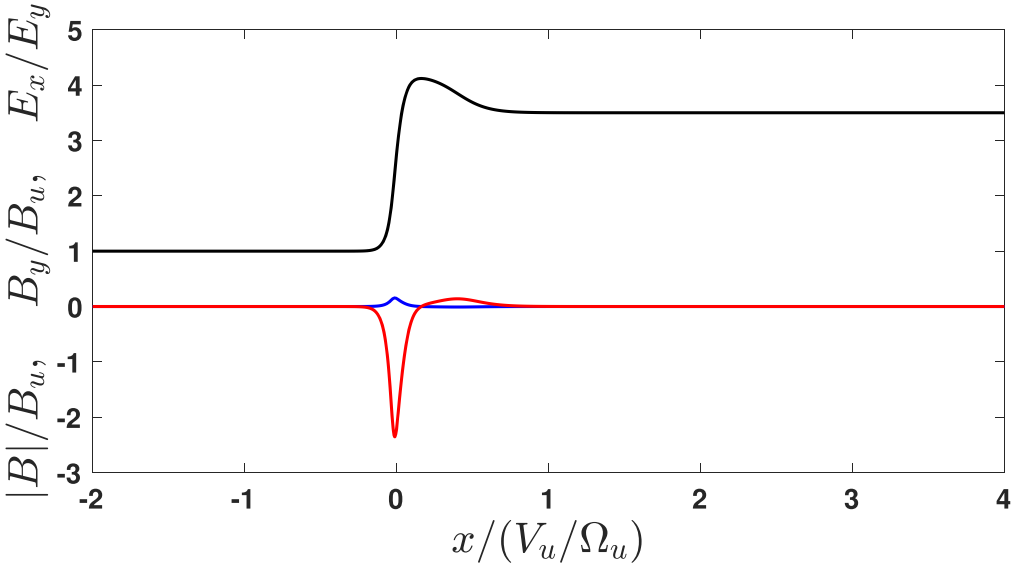

Figure 2. Magnetic field magnitude $|B|/B_u$ (black), noncoplanar magnetic field B_y/B_u (blue), and electric field E_x/E_y (red) for the model shock in the case $\theta_{Bn} = 85^\circ$.

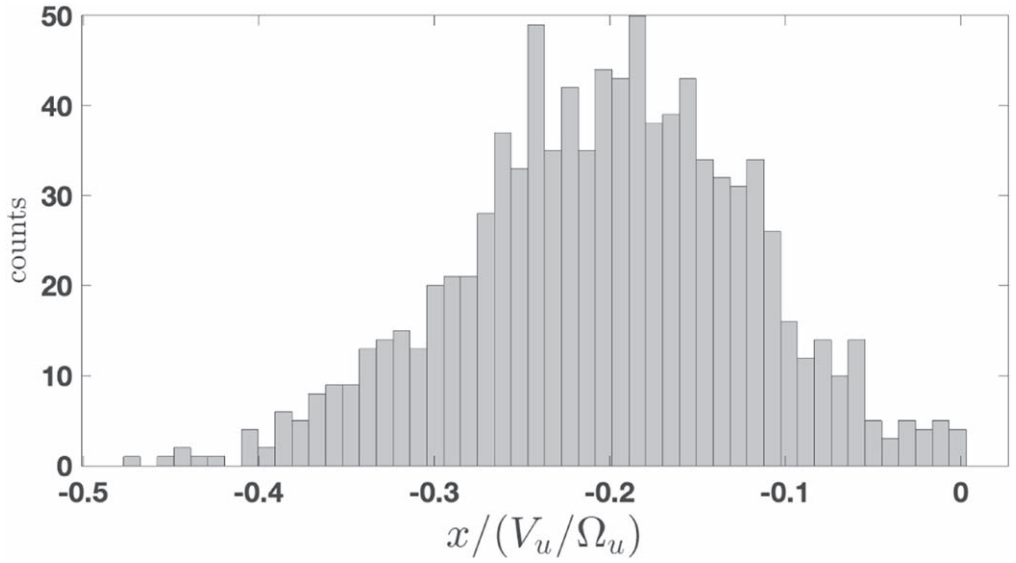

Figure 3. Histogram of the turning distances of reflected ions in the foot for $\theta_{Bn} = 85^\circ$.

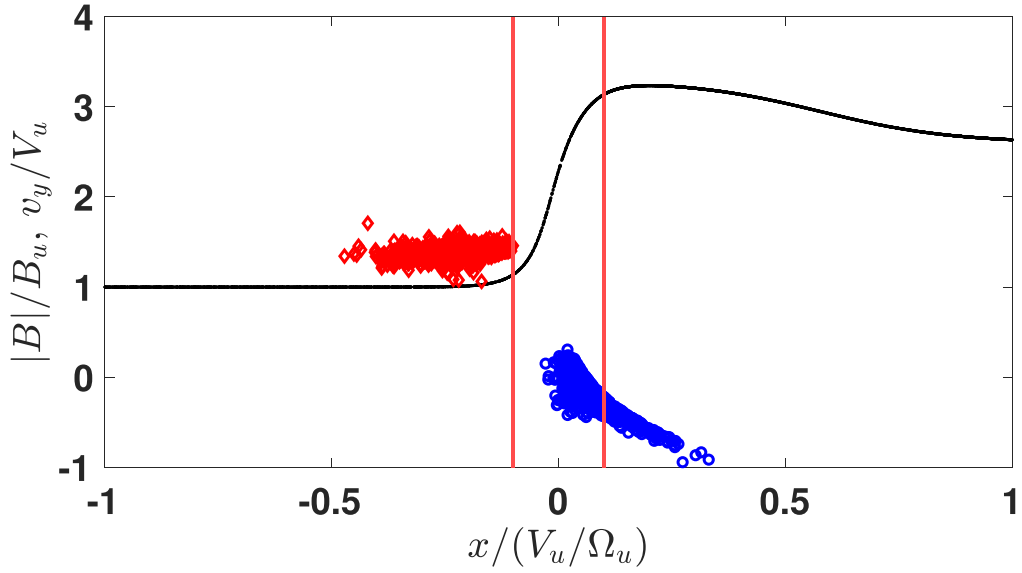

Figure 4. The shock magnetic profile (black), the positions and v_y of the reflected ions in the reflection point (blue), and the positions and v_y of the reflected ions in the turning point (red). The two red lines mark the beginning of the ramp up to the overshoot maximum.

$s \geqslant 1$ which results in a reflection of at least 50% of ions, which is too high in comparison with observations and numerical simulations. According to the observations of the terrestrial bow shock in the supercritical regime, the fraction of reflected ions is about 20% (Sckopke et al. 1983, 1990). This value is in agreement with the results of numerical simulations that also indicate that the fraction of reflected ions is significantly below 50% (e.g., ≈25%; Burgess et al. 1989), typically about 20% (Leroy et al. 1982)). For low upstream temperatures, reflection by the potential alone is valid only if the cross-shock potential is extremely large, $e\varphi_{\rm NIF} \approx m_p V_u^2/2$ (Wilkinson & Schwartz 1990). The observed cross-shock potentials are substantially lower (Schwartz et al. 1988; Dimmock et al. 2012). Figure 1 shows a histogram of the turning points for ions which are specularly reflected at a shock with the angle $\theta_{Bn} = 85°$ and Alfvénic Mach number $M = V_u/v_A = 4$. The incident distribution is Maxwellian with $\beta = 2v_T^2/v_A^2 = 0.5$. The normalized cross-shock potential between the upstream and the downstream region is $s = 0.6$. The red line marks the position of the upstream edge of the foot according to Gosling & Thomsen (1985).

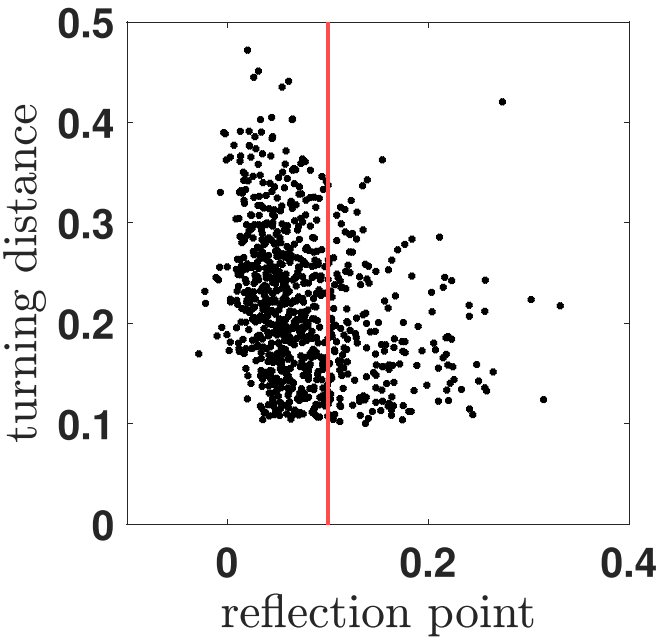

Figure 5. Relation of the turning distance to the position of the reflection point.

3. Nonspecular Reflection

Specular reflection is just a convenient approximation that ignores the fact that ions may be reflected within the ramp or behind it, thus spending some of their time in the region with an increasing magnetic field (Gedalin 1996, 2016). The reflection itself occurs at the point where $v_x = 0$. The inward and outward motion of the ion in the magnetic field of the ramp results in the changes of the two other components of the velocity before the reflected ion reappears again in the supposedly uniform upstream fields. In order to study ion reflection and foot width in real shocks, we perform numerical ion tracing in a model shock front. The model profile includes an overshoot. Since we are only interested in the dependence of the turning point on the shock parameters, there is no need to worry about the self-consistency of the model. For this analysis $M = 5$, $B_d/B_u = 3.5$, $B_{\rm max}/B_u \approx 4.2$, $s = 2e\varphi_{\rm NIF}/m_p V_u^2 = 0.4$, and $\beta = 0.5$. Note that the reflecting potential is the potential jump from the upstream region to the point at which the maximum magnetic field occurs, $s_m = s(B_{\rm max}/B_d)$. Figure 2 shows the magnetic field magnitude $|B|/B_u$ (black), noncoplanar magnetic field B_y/B_u (blue), and electric field E_x/E_y (red) for the model shock with $\theta_{Bn} = 85°$. Here x is along the shock normal and the motional electric field $E_y = V_u B_u \sin\theta_{Bn}/c$. In what follows we trace a particle population consisting of 40,000 ions (protons) with a Maxwellian distribution, and determine the location of the first and second turning points at which $v_x = 0$. The first turning point is the reflection point. For the reflected ions, the second turning point is in the upstream region, ahead of the ramp. Figure 3 shows a histogram of the turning distances of the reflected ions in the foot for $\theta_{Bn} = 85°$. While the specular reflection approach predicts the

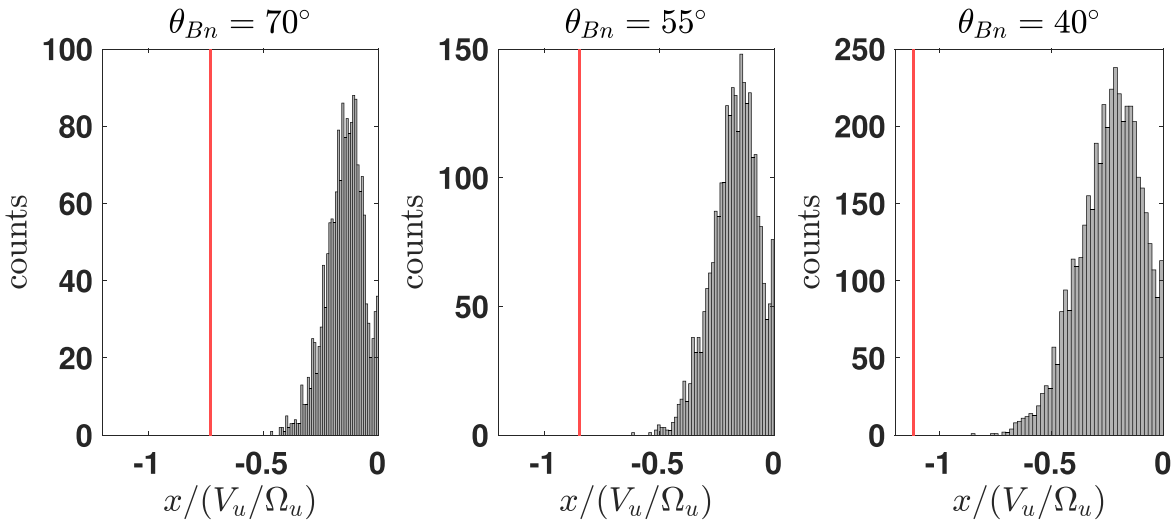

Figure 6. Histograms of the turning distances of reflected ions in the foot for three shock angles. The red line marks the position of the upstream edge of the foot according to Gosling & Thomsen (1985).

foot of $0.65(V_u/\Omega_u)$, the ion tracing shows that most of the turning distances are less than half of this value. The reflection is significantly nonspecular (Gedalin 2016), as is seen in Figure 4, which shows the positions and v_y of the reflected ions at the reflection point (blue), and the positions and v_y of the reflected ions in the second turning point (red), together with the magnetic field profile of the shock (black). The two red lines in Figure 4 mark the region approximately from the beginning of the ramp up to the overshoot maximum. A substantial fraction of the reflected ions are not reflected by the potential but continue to cross the ramp, gyrate in the post ramp magnetic field reversing their v_x, and then recross the ramp.

Figure 5 shows the relation of the turning distance to the position of the reflection point. The turning distance is the distance from the center of the ramp $x = 0$ to the second turning point of the reflected ion. All ions to the right of the red line are not reflected by the potential.

Figure 6 shows histograms of the turning distances of reflected ions for three shock angles. Only a few percent of the reflected ions have turning distances, which is approximately half of the value suggested by Gosling & Thomsen (1985), while most of them have smaller turning distances. The maximum turning distance increases with decreasing values of θ_{Bn}.

Figure 7 shows histograms of the turning distances of reflected ions in the foot for $\theta_{Bn} = 70°$, $\beta = 0.3$, and for three values of the cross-shock potential $s = 0.4,\ 0.5,\ 0.6$. The efficiency of reflection and the turning distance decrease rapidly with the decrease of the potential. Figure 8 shows the histograms of the turning points of reflected ions in the foot for $\theta_{Bn} = 70°$, $s = 0.5$, and three values of $\beta = 0.2,\ 0.4,\ 0.6$. The efficiency of reflection and the turning distance decrease rapidly with the decrease of β. To be more precise, the control parameter is $v_T \Big/ V_u = \frac{\sqrt{\beta/2}}{M}$ (Gedalin 1996, 2016).

4. Discussion

Among a large number of heliospheric collisionless shocks observations by various spacecraft, one of the most comprehensive studies (maybe the most comprehensive) has been conducted by Scudder et al. (1986a, 1986c, 1986b). This study examined in detail the crossing of a quasi-perpendicular part of the terrestrial bow shock on 07.11.1977 by the ISEE-1,2 spacecraft. The parameters of the shock were (Scudder et al. 1986c): the fast magnetosonic Mach number $M_{ms} = 3.8 \pm 0.4$ and $\theta_{Bn} = 76° \pm 4°$. The shock velocity along the shock normal in the spacecraft frame was inferred from two spacecraft measurements as $7.1\ \mathrm{km\,s^{-1}}$, while the duration of the foot traversal was 24 s. This leads to the estimated foot width being about 170 km. The upstream ion convective gyroradius was estimated to be 560 km. Thus, the foot width for this supercritical quasi-perpendicular shock is about $0.3(V_u/\Omega_u)$. According to the Gosling & Thomsen (1985) model, the foot width for $\theta_{Bn} = 76°$ should be about $0.7(V_u/\Omega_u)$. The observed foot width is less than half of this prediction but is consistent with the findings of the current study.

Currently only in the heliosphere, collisionless shocks can be subjected to in situ observations that enable the validation of physical models of shock-related processes. Range of parameters of collisionless shocks in the heliosphere results in a diversity of physical processes occurring at the front. Therefore, in addition to the terrestrial bow shock that can be subjected to in situ measurements by fleets of multispacecraft missions, all other collisionless shocks that are observed in other regions of the heliosphere should also be subjected to thorough investigations. Planetary and interplanetary missions do not have the luxury of multipoint observations by closely spaced satellites and face the problem of how to distinguish between spatial and temporal variations and identify spatial scales of observed phenomena. Spatial scales of shock front regions are central to the dynamical processes at the front as they are directly related to processes involved in the formation of a shock. In addition, spatial scales of electric and magnetic fields within the shock affect the process of particles thermalization at the shock front (e.g., Balikhin et al. 1993; Balikhin & Gedalin 1994). For single spacecraft missions, the methodology based on the width of the foot enables identification of the relative spacecraft shock velocity and spatial scales of more complex shock regions of the shock front such as the magnetic ramp.

The results presented in this study manifest the physics of ion reflection at the shock front (Gedalin 1996, 2016). The basic difference between the processes of specular reflections of previous models and nonspecular reflection is the role of the

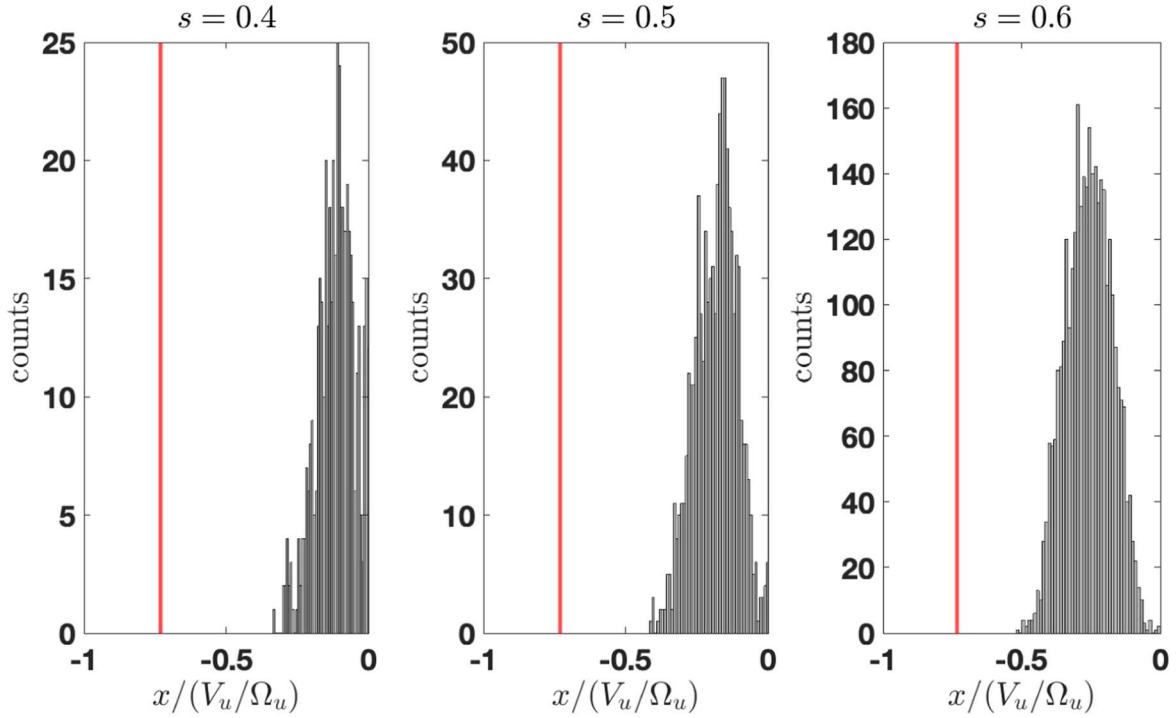

Figure 7. Histograms of the turning distances of the reflected ions in the foot for $\theta_{Bn} = 70°$, $\beta = 0.3$, and three values of the cross-shock potential $s = 0.4$, 0.5, 0.6. The red line marks the position of the upstream edge of the foot according to Gosling & Thomsen (1985).

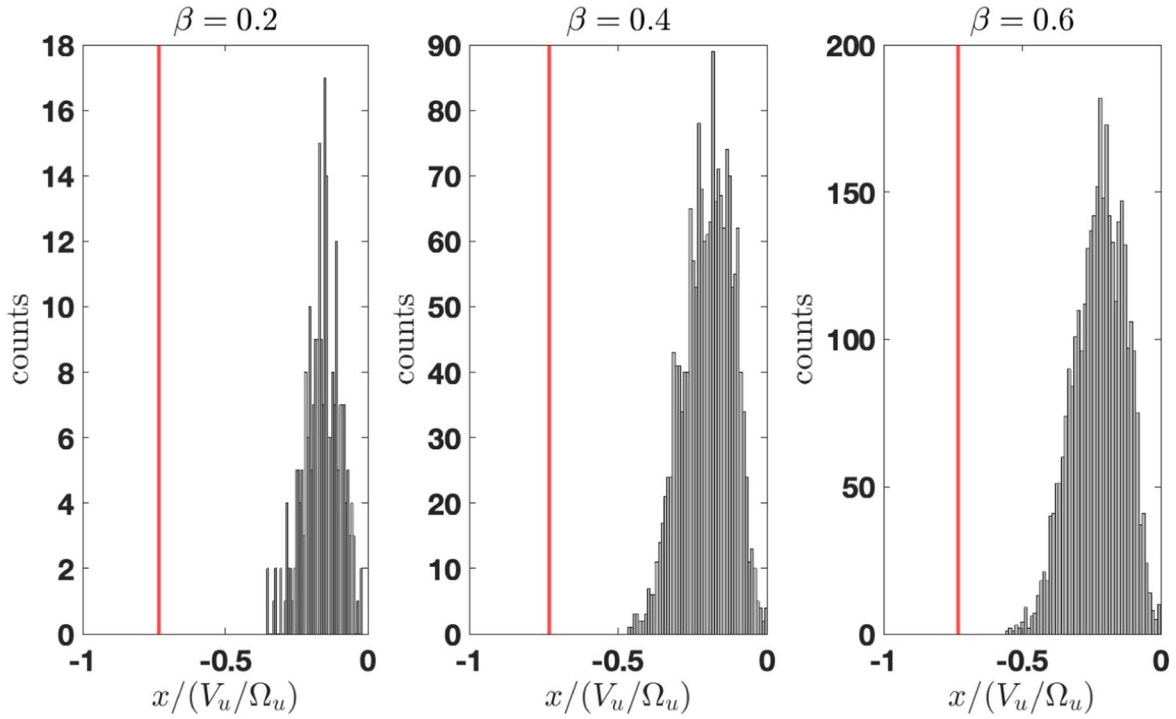

Figure 8. Histograms of the turning points of reflected ions in the foot for $\theta_{Bn} = 70°$, $s = 0.5$, and three values of $\beta = 0.2$, 0.4, 0.6. The red line marks the position of the upstream edge of the foot according to Gosling & Thomsen (1985).

magnetic field in this process. Specular reflection models overlook the significant role of the magnetic field in ion reflection. In the case of a cold plasma flow, reflection that is solely based on the electrostatic potential requires $s = 2e\phi/mV_u^2 \approx 1$. In such a case, the speed of the reflected ions prior to reflection is close to the upstream bulk velocity and the Gosling & Thomsen (1985) model can be used to estimate their turning point and the width of the foot region. In reality s is lower and, as a result of both the magnetic field and electrostatic potential, nonspecular reflection occurs. The velocities of reflected particles prior to reflection are lower than the upstream bulk velocity. Their effective gyro-radii are smaller than those calculated using the upstream bulk velocity, resulting in the more narrow foot region.

5. Conclusions

The width of the foot increases with decreasing the shock angle, with increasing the cross-shock potential, and with increasing upstream β. The foot width is substantially smaller than the width predicted by the simplified specular reflection model (Gosling & Thomsen 1985). The real width may be as small as half of the width in case of a specular reflection. Inferring shock speed on the basis of the widely used expression may lead to 100% errors.

M.B. was partially supported by the UK STFC ST/R000697/1 grant. M.G. was partially supported by the European Unions Horizon 2020 research and innovation program under grant agreement No. 101004131. The authors are grateful to Simon Walker for useful discussions.

ORCID iDs

Michael Balikhin https://orcid.org/0000-0002-8110-5626
Michael Gedalin https://orcid.org/0000-0003-1236-4787

References

Balikhin, M., & Gedalin, M. 1994, GeoRL, 21, 841
Balikhin, M., Gedalin, M., & Petrukovich, A. 1993, PhRvL, 70, 1259
Balikhin, M. A., Zhang, T. L., Gedalin, M., Ganushkina, N. Y., & Pope, S. A. 2008, GeoRL, 35, L01103
Burgess, D., Wilkinson, W. P., & Schwartz, S. J. 1989, JGR, 94, 8783
Dimmock, A. P., Balikhin, M. A., Krasnoselskikh, V. V., et al. 2012, JGR, 117, 02210
Gedalin, M. 1996, JGR, 101, 4871
Gedalin, M. 2016, JGR, 121, 10
Gedalin, M. 2019, FrP, 7, 692
Gedalin, M., Zhou, X., Russell, C. T., Drozdov, A., & Liu, T. Z. 2018, JGR, 123, 8913
Gosling, J. T., & Thomsen, M. F. 1985, JGR, 90, 9893
Hobara, Y., Balikhin, M., Krasnoselskikh, V., Gedalin, M., & Yamagishi, H. 2010, JGR, 115, 11106
Krasnoselskikh, V., Balikhin, M., Walker, S. N., et al. 2013, SSRv, 178, 535
Leroy, M. M., Winske, D., Goodrich, C. C., Wu, C. S., & Papadopoulos, K. 1982, JGR, 87, 5081
Livesey, W. A., Kennel, C. F., & Russell, C. T. 1982, GeoRL, 9, 1037
Livesey, W. A., Russell, C. T., & Kennel, C. F. 1984, JGR, 89, 6824
Moses, S. L., Coroniti, F. V., Kennel, C. F., et al. 1985, GeoRL, 12, 183
Phillips, P. E., & Robson, A. E. 1972, PhRvL, 29, 154
Pope, S. A. 2020, JGR, 125, A028256
Pope, S. A., Gedalin, M., & Balikhin, M. A. 2019, JGR, 165, 3
Russell, C. T., Jian, L. K., Blanco-Cano, X., & Luhmann, J. G. 2009, GeoRL, 36, 03106
Schwartz, S. J., Thomsen, M. F., Bame, S. J., & Stansberry, J. 1988, JGR, 93, 12923
Schwartz, S. J., Thomsen, M. F., & Gosling, J. T. 1983, JGR, 88, 2039
Sckopke, N., Paschmann, G., Bame, S. J., Gosling, J. T., & Russell, C. T. 1983, JGR, 88, 6121
Sckopke, N., Paschmann, G., Brinca, A. L., Carlson, C. W., & Luehr, H. 1990, JGR, 95, 6337
Scudder, J., Mangeney, A., Lacombe, C., et al. 1986a, JGR, 91, 11075
Scudder, J., Scudder, J. D., Aggson, T. L., et al. 1986b, JGR, 91, 11053
Scudder, J. D., Aggson, T., Aggson, T. L., et al. 1986c, JGR, 91, 11019
Wilkinson, W. P., & Schwartz, S. J. 1990, P&SS, 38, 419
Woods, L. 1971, PlPh, 13, 289